

Efficient infrared thermal emitters based on low-albedo polaritonic meta-surfaces

Burton Neuner, Chihhui Wu, Gregory Ten Eyck, Michael Sinclair, Igal Brener et al.

Citation: *Appl. Phys. Lett.* **102**, 211111 (2013); doi: 10.1063/1.4808086

View online: <http://dx.doi.org/10.1063/1.4808086>

View Table of Contents: <http://apl.aip.org/resource/1/APPLAB/v102/i21>

Published by the [American Institute of Physics](http://www.aip.org).

Additional information on *Appl. Phys. Lett.*

Journal Homepage: <http://apl.aip.org/>

Journal Information: http://apl.aip.org/about/about_the_journal

Top downloads: http://apl.aip.org/features/most_downloaded

Information for Authors: <http://apl.aip.org/authors>

ADVERTISEMENT



Improve your Images with Minus K's
Negative-Stiffness Vibration Isolation

Workstations & Optical Tables



Custom Applications



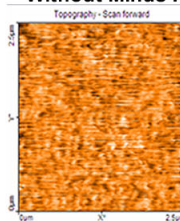
Bench Top Isolators



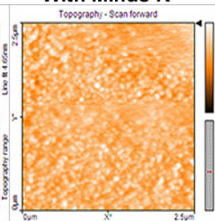
Multi Isolator Systems



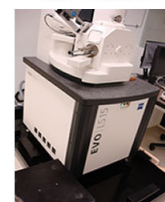
Without Minus K



With Minus K



Floor Platforms



Efficient infrared thermal emitters based on low-albedo polaritonic meta-surfaces

Burton Neuner III,¹ Chihhui Wu,¹ Gregory Ten Eyck,² Michael Sinclair,² Igal Brener,² and Gennady Shvets^{1,a)}

¹Department of Physics, University of Texas at Austin, Austin, Texas 78712, USA

²Sandia National Laboratories, New Mexico, PO Box 5800, Albuquerque, New Mexico 87185-1082, USA

(Received 17 September 2012; accepted 12 May 2013; published online 31 May 2013)

A low-albedo all-semiconductor meta-surface with spectrally selective absorption peaks is demonstrated. By engineering the dimensions and shapes of the semiconductor antennas comprising the meta-surface, simultaneous reduction of reflectivity and enhancement of absorption are accomplished by controlling their electric and magnetic resonances. Thermal emissivity of the silicon carbide-based meta-surface is experimentally measured and found in agreement with both absorption measurements and theoretical predictions. © 2013 AIP Publishing LLC.

[<http://dx.doi.org/10.1063/1.4808086>]

Mid-infrared (IR) and far-infrared radiation find numerous applications in the areas of national security,¹ communications, thermal photovoltaics (TPVs), biochemical sensing/spectroscopy,² and even art history. Of particular interest are spectrally selective thermal emitters that are important for the structural characterizations of nanoscale molecular and biological samples,³ partial-coherence tomography of bio-engineered tissues,⁴ and the development of efficient thermoelectric radiation sources. Single-element, spectrally selective IR emitters based on plasmonic⁵ and semiconductor^{6,7} antennas have been experimentally demonstrated. Practical applications such as TPVs, however, require high-infrared-energy fluxes that cannot be obtained from a single antenna emitter.

In this letter, we report the results of theory, design, fabrication, and optical characterization of large-area meta-surfaces (MSs) for thermal emission comprised of IR semiconductor antennas. The attraction of thermal emitters based on semiconductor antennas, which are also known in the literature as dielectric resonator antennas (DRAs)^{8,9} because they do not rely on conducting electrons, is three-fold. First, optical properties of many high-index semiconductors are essentially frequency-independent across broad spectral range, unlike those of plasmonic structures. For example, the refractive index of germanium (Ge) changes by less than 6% in the relatively broadband $2\ \mu\text{m} < \lambda < 10\ \mu\text{m}$ infrared spectral range. Second, the ability to affect the refractive index of semiconductors by introducing free carriers enables either active or passive control of their optical properties. Third, high conductivity of doped semiconductors enables their electric heating.

Using methodology from the field of metamaterials, we show that DRAs based on high-index semiconductors can be engineered to overcome one of the major challenges to designing spectrally selective resonant surfaces: high albedo (reflectivity, R), which prevents the peak emissivity from approaching the black-body limit. These 3D antennas, which can be fabricated from any semiconductor possessing a

sufficiently large dielectric permittivity, rely on Mie-type resonances, and therefore lengths must be larger than λ/n . Given that the meta-surface should have sub- λ pitch ($< \lambda/2$) and even smaller antenna sizes, we concentrate on dielectrics with $\epsilon \geq 10$. Antennas are engineered to spectrally match their electric and magnetic responses. The resulting meta-surface exhibits an albedo below that of the underlying substrate and surrounding unpatterned antenna material, as well as spectrally narrow absorption peaks^{10,11} with resonant frequencies tunable by changing antenna geometry. Therefore, the spectrally selective emissivity of such MSs at temperature T , given by $E_{MS}(\lambda, T) = E_{BB}(\lambda, T) \times A(\lambda)$ according to the Kirchhoff's Law, can approach the black-body emissivity $E_{BB}(\lambda, T)$ if the absorptivity $A(\lambda) > 1 - R(\lambda)$ approaches unity for at least some values of λ .

The importance of reducing meta-surface reflectivity is first illustrated by theory and modeling in Fig. 1, where we plot reflection and absorption ($A = 1 - R - T$) of an array of 2D, heavily doped Ge nanowires illuminated by y -polarized light. The permittivity of Ge is represented by the Drude model¹² $\epsilon_{\text{Ge}}(\omega) = 16 - \omega_p^2 / (\omega(\omega + i\gamma))$, where $m_{\text{eff}} = 0.15m_e$, $N = 2 \times 10^{18}\ \text{cm}^{-3}$, and $\gamma^{-1} = 10^{-14}\ \text{s}$. The wires are infinitely long in the y -direction and have an x - z cross-section of $2.25\ \mu\text{m} \times 1.05\ \mu\text{m}$; for simplicity, the substrate is not included. The long-antenna array exhibits very high reflectivity across the spectrum, resulting in small absorbance, as evident in Fig. 1(b). To understand the origin of high reflectivity, we numerically calculated the eigenmodes and eigenfrequencies of an array of long antennas as a function of the wave-number $\beta_y(\lambda)$ along the antenna. For small values of β_y , the two eigenmodes shown in Fig. 1(a) correspond to the (transverse magnetic) TM_0 (blue) and TM_1 (green) modes.⁶ Undesirable broadband reflectivity from long antennas originates from a strong *electric* resonance produced by the TM_0 mode, and is further increased by the *magnetic* resonance produced by the TM_1 mode. Significantly higher absorption would result from making the strengths and spectral positions of the magnetic and electric resonances similar or identical.

To explore how increased absorption can be accomplished, we consider the spectral positions and field profiles

^{a)}Electronic mail: gena@physics.utexas.edu

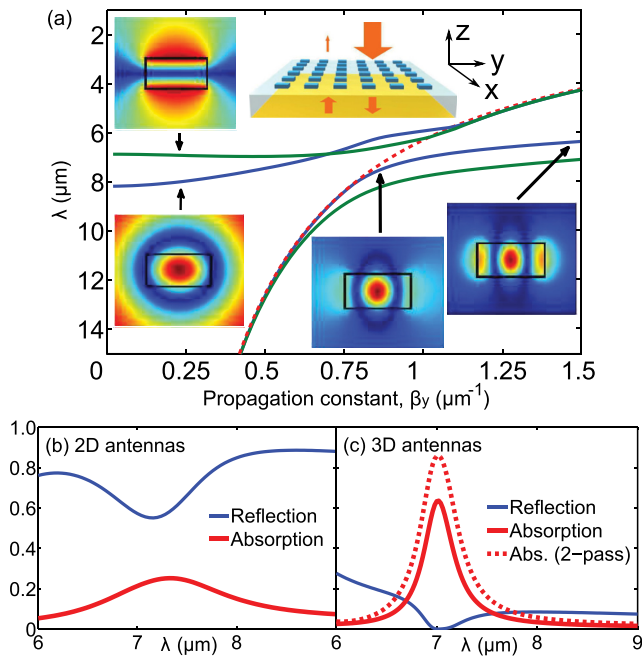


FIG. 1. Reflectivity reduction and absorptivity enhancement of a semiconductor (Ge) antenna meta-surface. (a) Dispersion relations $\lambda(\beta_y)$ of TM_0 (blue lines) and TM_1 (green lines) modes of an infinitely long Ge nanowire (cross section: $L_x \times L_z = 2.25 \mu\text{m} \times 1.05 \mu\text{m}$). Red dashed line: the light line $\lambda \equiv 2\pi/\beta_y$. Color-coded insets: $|E_y|$ for the TM_0/TM_1 modes. Upper middle inset: schematic of a double-pass array with a reflective ground plate. Simulated reflection (blue) and single/double-pass absorption (red) for (b) 2D and (c) 3D antennas.

of eigenmodes for large $\beta_y > 2\pi/\lambda$. Such modes can be coupled to the incident radiation by breaking the translational symmetry of the nanowires in the y -direction by segmenting them into half-wavelength antennas of the length $L_y \approx \pi/\beta_y$. Below we preserve the nomenclature of TM-dominant and transverse electric (TE)-dominant modes despite their hybridization for finite β_y . As β_y increases, the electric field distribution of the TM_1 mode remains essentially the same while the TM_0 mode becomes multi-nodal, thereby reducing its electric dipole strength. At the same time, the spectral position of the TM_0 mode blue-shifts. By judicious choice of the antenna length, the electric and magnetic resonances can be made to spectrally overlap, resulting in better-matched impedance, much lower R , and higher A when compared to the long-antenna array. The result of length optimization is shown in Fig. 1(c), where simulated single/double pass absorption (red lines) and interfacial reflection (blue line) from finite-sized antennas with $L_y = 2.25 \mu\text{m}$ are plotted. By spectrally overlapping the electric and magnetic resonances, R from the MS comprised of 3D Ge antennas is reduced ten-fold compared with the nanowire array. Furthermore, A exceeds 65% for single-pass and 90% for double-pass (mirror-backed) propagation.

For experimental realization, we chose a different semiconductor, silicon carbide (SiC), which has already found utility as the material for IR index sensors,¹³ super-lenses,¹⁴ and other photonic structures.^{6,15–17} In close spectral proximity to $\lambda \approx \lambda_{TO} = 12.5 \mu\text{m}$, SiC exhibits the requisite large $\Re\epsilon$, as well as finite intrinsic $\Im\epsilon$ without any need for doping. Thus, alongside doped Ge, Si, and most III-V semiconductors, SiC is an excellent platform for testing the concept of

high-absorptivity semiconductor meta-surfaces. Also important for SiC's potential for thermal emission applications is its ability to withstand very high temperatures ($>1000^\circ\text{C}$). Long SiC whiskers have been proposed as spectrally engineered thermal emission sources.¹⁷ Therefore, demonstrating the experimental capability of fabricating large arrays of sub-wavelength 3D SiC antennas is yet another objective of this letter. Although less relevant for the present study, SiC's optical properties in the so-called *reststrahlen* spectral region, $\lambda_{TO} > \lambda > \lambda_{LO} \approx 10.47 \mu\text{m}$, where $\epsilon < 0$ as shown in Fig. 2(b), also make it an interesting platform for investigating plasmonic antenna arrays in the mid-IR spectrum.

The 625-nm-thick polycrystalline 3C-SiC layer¹⁸ was grown on a double-polished Si(100) wafer. The structure was patterned using contact lithography. The inverse pattern was used with liftoff to create an etch mask of 100-nm-thick Ni/Cr islands. The SiC was etched at room temperature with SF_6 using an Unaxis inductively coupled rf plasma etch system. A 10% over-etch ensured complete removal of SiC and lead to the 300-nm Si isotropic undercut etch (visible in Fig. 2(a)). The total area of the array is a full $9 \text{mm} \times 9 \text{mm}$, and unit cell dimensions are shown in Fig. 2(c).

Direct measurements of moderate-temperature (100°C – 150°C) emissivity were carried out using a variable-angle directional emissometer (VADE).¹⁹ As illustrated in Fig. 3(f), the system uses a Fourier transform IR (FTIR) spectrometer to compare the unpolarized thermal emission of the sample $E_{MS}(\lambda, T)$ to a known reference $E_{BB}(\lambda, T)$ on a common heated stage. The reference is made from the same substrate as the sample but coated with a spectrally flat, high-emissivity paint. The normalized emissivity spectrum shown in Fig. 3(e) exhibits three clear peaks: one in the high-index spectral region of $\epsilon_{\text{SiC}} \gg 1$ and two more in the plasmonic region of $\epsilon_{\text{SiC}} < 0$.

To verify the accuracy of the emissivity measurement, an independent set of polarized transmission and reflection spectra of the SiC meta-surface was collected in the $9 \mu\text{m}$ – $15 \mu\text{m}$ spectral range with a Thermo Scientific Continuum microscope coupled to a Nicolet 6700 FTIR spectrometer using s -polarized radiation. Polarized-spectroscopy schematics using E -field parallel (E_{\parallel}) and perpendicular (E_{\perp}) to

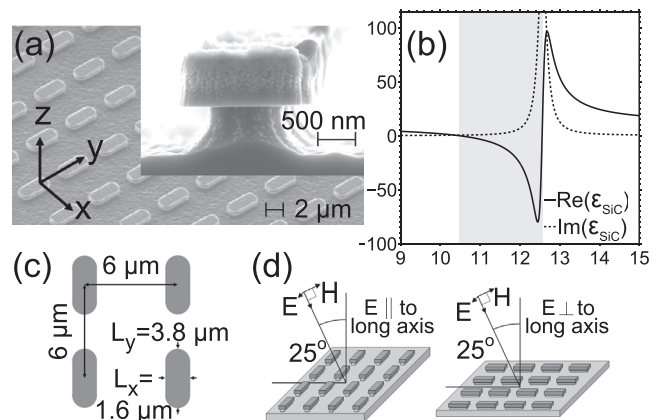


FIG. 2. Large-area SiC antenna meta-surfaces. (a) Scanning electron micrographs of the $6\text{-}\mu\text{m}$ -pitch antenna array and a single SiC antenna. (b) SiC permittivity, with $\epsilon_{\text{SiC}} < 0$ shaded. (c) Physical dimensions of the SiC antenna arrays. (d) Illumination schematics for s -polarized E -field aligned parallel (\parallel) and perpendicular (\perp) to the long axis.

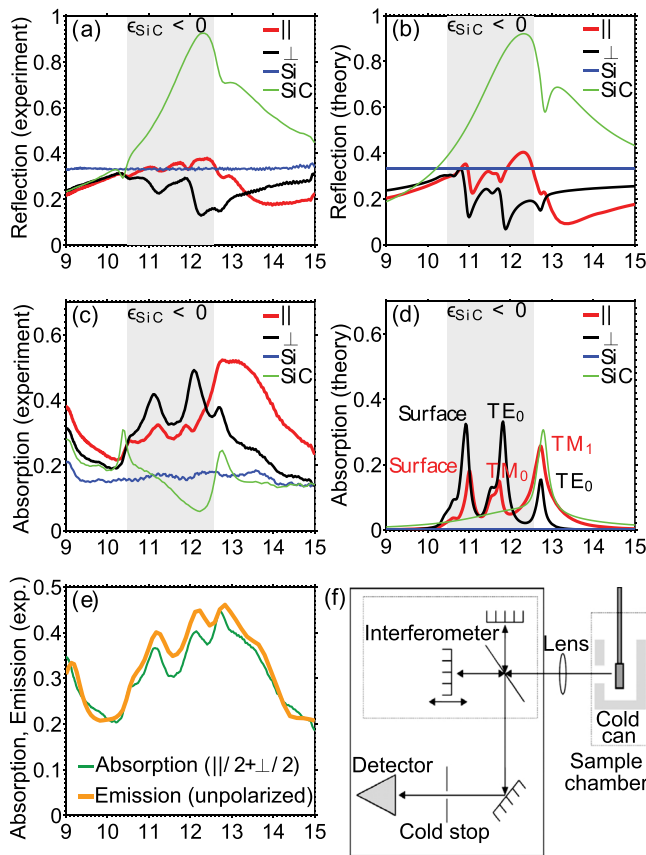


FIG. 3. Spectral properties of large-area meta-surfaces based on SiC antennas. ((a) and (b)) Reflection and ((c) and (d)) absorption spectra. (a) and (c) Experiments are compared to ((b) and (d)) theory. Resonance peaks are labeled in (d) according to the prevailing nature of the resonant mode. TM-dominant modes correspond to E_{\parallel} polarization, and TE-dominant modes to E_{\perp} . Surface modes contribute to both polarizations. (e) Unpolarized thermal emission (schematic in (f)) from the array is compared to polarization-averaged absorption (data from (c)).

the antenna's long axis are shown in Fig. 2(d). Reflection and absorption spectra are plotted in Figs. 3(a) and 3(c), respectively. The albedo of the meta-surface is reduced below that of smooth SiC for both polarizations, as evident in Fig. 3(a).

Multiple absorption peaks greatly exceeding the baseline absorption in the Si substrate are clearly observed in Fig. 3(c). The SiC meta-surface exhibits strong absorptivity (up to 50%) for both polarizations and for both signs of ϵ_{SiC} , which is a factor of 3 higher than from the substrate, and more than twice that from smooth SiC. The comparison between unpolarized emissivity and absorptivity in Fig. 3(e) shows excellent agreement between these two independent measurements. Slight modification of the structure (e.g., patterning arrays on both sides of the substrate and placing a reflecting metallic structure behind the back surface, thus, resulting in multiple passages through the antenna arrays) would enable spectrally sharp emissivity with peak values closer to that of a black body.

To identify and understand the physical nature of the multiple absorption peaks, finite element method (FEM) numerical simulations of SiC meta-surfaces were performed with COMSOL software. The 3D simulation domain contains a single SiC antenna, a Si pedestal, and a Si substrate

($\epsilon_{\text{Si}} = 11.6$) with periodic boundary conditions. The permittivity of SiC used in the simulation is given by $\epsilon_{\text{SiC}}(\omega) = \epsilon_{\infty}(\omega_{\text{LO}}^2 - \omega^2 + i\gamma\omega)/(\omega_{\text{TO}}^2 - \omega^2 + i\gamma\omega)$,²⁰ where $\epsilon_{\infty} = 6.7$, the longitudinal optical phonon frequency $\omega_{\text{LO}} \equiv 2\pi c/\lambda_{\text{LO}} = 955 \text{ cm}^{-1}$, the transverse optical phonon frequency $\omega_{\text{TO}} = 796 \text{ cm}^{-1}$, and the damping rate $\gamma = 10 \text{ cm}^{-1}$. Simulation results are shown in Figs. 3(b) and 3(d); non-complex ϵ_{Si} leads to $A_{\text{Si}} = 0$. The numerically obtained absorption peaks and the reduced albedo match the experimentally obtained results shown in Figs. 3(a) and 3(c). Discrepancies between simulation and experiment arise from three sources: (i) Si wafer absorption, which can be mitigated through the use of intrinsic, undoped Si, (ii) inhomogeneous spectral broadening from lithographic and etching imperfections, which can be improved with advanced fabrication, and (iii) angular averaging from collection optics, which can be reduced using advanced lower-numerical-aperture optics.

With good agreement between experiments and simulations established, we used simulation results such as the complex transmission/reflection coefficients and electromagnetic field profiles to assign physical meaning to various absorption peaks. We start with the high-index dielectric portion ($\lambda > \lambda_{\text{TO}}$) of the spectrum, where absorption peaks are found around $\lambda \approx 12.7 \mu\text{m}$ for both polarizations. For \parallel polarization, the absorption peak of the SiC meta-surface corresponds to the excitation of the TM_1 -dominant magnetic resonance shown in Fig. 4(f), which is conceptually similar to the one predicted for Ge-based meta-surfaces shown in Fig. 1(a). The effective ϵ and μ of the SiC metamaterial calculated from the scattering matrix and plotted in Figs. 4(c) and 4(d) clearly show that the reduced R and enhanced A originate from a good matching between electric and

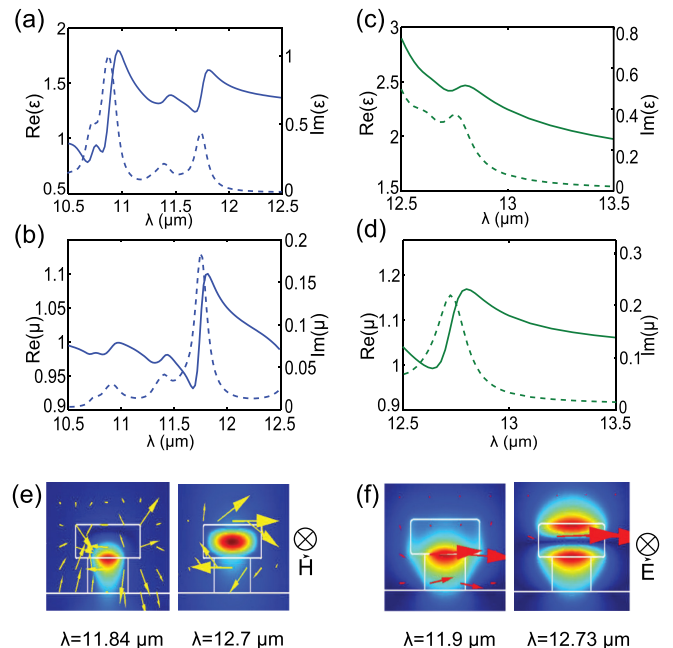


FIG. 4. Theoretical interpretation of SiC meta-surface resonances. Real (solid lines) and complex (dashed lines) components of the constitutive parameters of the meta-surface for E_{\perp} polarization in plasmonic spectral region: (a) permittivity ϵ and (b) permeability μ . (c) and (d) ϵ and μ for E_{\parallel} polarization in the high-index dielectric spectral region. (e) Resonant modes with E_{\perp} polarization. Color: $|H_y|$, yellow arrows: E. (f) Modes with E_{\parallel} polarization. Color: $|E_y|$, red arrows: H.

magnetic responses. A considerably weaker absorption peak corresponding to the TE₀-dominant magnetic resonance⁶ (shown in Fig. 4(e)) is also predicted at $\lambda = 12.7 \mu\text{m}$ for E_⊥ polarization.

In the plasmonic spectral region ($\lambda_{\text{TO}} > \lambda > \lambda_{\text{LO}}$), the SiC meta-surface exhibits absorption peaks around $\lambda = 11.8 \mu\text{m}$ for both polarizations. Because the ⊥ polarization of the electric field yields much stronger absorption peaks, we concentrate below on that polarization. The color-coded magnetic field profile at $\lambda = 11.84 \mu\text{m}$ plotted in Fig. 4(e) indicates the excitation of a TE₀-like resonance. The spatial distribution of the magnetic field is predicted to be highly asymmetric because of the asymmetric nature of the SiC antenna ($\epsilon_{\text{SiC}} < 0$) sitting on top of Si pedestals ($\epsilon_{\text{Si}} > 0$). As shown in Fig. 4(e), the field is strongly concentrated at the SiC/Si interface that is responsible for the asymmetry. The ϵ and μ coefficients were extracted according to the standard procedure²¹ and plotted in Figs. 4(a) and 4(b). Once again, good matching between electric and magnetic responses of the meta-surface is responsible for the reduced reflectivity of the SiC meta-surface. We note in passing that the third A peak near $\lambda \approx 10.9 \mu\text{m}$ corresponds to the excitation of antenna surface resonances, which are beyond the scope of this work. Although the plasmonic regime of SiC is less relevant to the present study that focused on meta-surfaces comprised of *high-index semiconductors*, it is nevertheless an interesting spectral range for exploring plasmonic metamaterials and antennas.

In conclusion, we have demonstrated the engineering of low-albedo meta-surfaces that are based on high-index semiconductors and are capable of spectrally selective thermal emission with peak emissivity approaching that of black-body radiation. Low albedo, which is the key design feature enabling high peak emissivity, was achieved by 3D antenna design that discriminates between scattering and absorbing resonances of the individual antennas. The experimentally realized meta-surface was comprised of 3D engineered SiC antennas on a Si substrate. The absolute, room-temperature, spectrally selective emissivity of the meta-surface was directly measured and approached 50% of the black-body limit. Straightforward modifications of the design, such as introducing meta-surfaces to both substrate sides, can increase peak emissivity even further. Despite the sharp absorption resonances, the experimentally measured albedo of the meta-surface was below that of the smooth antenna

material and underlying substrate for nearly all frequencies. This design methodology paves the way to exciting applications of semiconductor meta-surfaces as highly efficient, spectrally narrow thermal emitters.

This work was supported by Sandia National Laboratories New Mexico, the U.S. Air Force Office of Scientific Research (AFOSR) MURI Grant No. FA-9550-08-1-0394, and by the Office of Naval Research (ONR) Grant No. N00014-10-1-0929.

- ¹M. C. Kemp, P. F. Taday, B. E. Cole, J. A. Cluff, A. J. Fitzgerald, and W. R. Tribe, *Proc. SPIE* **5070**, 44 (2003).
- ²R. Adato, A. A. Yanik, J. J. Amsden, D. L. Kaplan, F. G. Omenetto, M. K. Hong, S. Erramilli, and H. Altug, *Proc. Natl. Acad. Sci. U.S.A.* **106**, 19227 (2009).
- ³R. Hillenbrand, *Ultramicroscopy* **100**, 421 (2004).
- ⁴C. S. Colley, J. C. Hebden, D. T. Delpy, A. D. Cambrey, R. A. Brown, E. A. Zibik, W. H. Ng, L. R. Wilson, and J. W. Cockburn, *Rev. Sci. Instrum.* **78**, 123108 (2007).
- ⁵L. J. Klein, H. F. Hamann, Y.-Y. Au, and S. Ingvarsson, *Appl. Phys. Lett.* **92**, 213102 (2008).
- ⁶J. A. Schuller, T. Taubner, and M. L. Brongersma, *Nature Photon.* **3**, 658 (2009).
- ⁷L. Cao, P. Fan, A. P. Vasudev, J. S. White, Z. Yu, W. Cai, J. A. Schuller, S. Fan, and M. L. Brongersma, *Nano Lett.* **10**, 439 (2010).
- ⁸N. Petosa, R. Simons, A. Siushansian, A. Ittipiboon, and C. Michel, *IEEE Trans. Antennas Propag.* **48**, 738 (2000).
- ⁹*Dielectric Resonator Antennas*, edited by K. M. Luk and K. W. Leung (Research Studies Press Ltd., Hertfordshire, UK, 2002).
- ¹⁰H. Tao, N. I. Landy, C. M. Bingham, X. Zhang, R. D. Averitt, and W. J. Padilla, *Opt. Express* **16**, 7181 (2008).
- ¹¹J. A. Mason, S. Smith, and D. Wasserman, *Appl. Phys. Lett.* **98**, 241105 (2011).
- ¹²R. Soref, J. Hendrickson, and J. W. Cleary, *Opt. Express* **20**, 3814 (2012).
- ¹³B. Neuner III, D. Korobkin, C. Fietz, D. Carole, G. Ferro, and G. Shvets, *J. Phys. Chem. C* **114**, 7489 (2010).
- ¹⁴T. Taubner, D. Korobkin, Y. Urzhumov, G. Shvets, and R. Hillenbrand, *Science* **313**, 1595 (2006).
- ¹⁵J.-J. Greffet, R. Carminati, K. Joulain, J.-P. Mulet, S. Mainguy, and Y. Chen, *Nature* **416**, 61 (2002).
- ¹⁶Y. A. Urzhumov, D. Korobkin, B. Neuner III, C. Zorman, and G. Shvets, *J. Opt. A, Pure Appl. Opt.* **9**, S322 (2007).
- ¹⁷J. A. Schuller, R. Zia, T. Taubner, and M. L. Brongersma, *Phys. Rev. Lett.* **99**, 107401 (2007).
- ¹⁸M. B. J. Wijesundara, G. Valente, W. R. Ashurst, R. T. Howe, A. P. Pisano, C. Carraro, and R. Maboudian, *J. Electrochem. Soc.* **151**, C210 (2004).
- ¹⁹A. R. Ellis, H. M. Graham, M. B. Sinclair, and J. C. Verley, *Proc. SPIE* **7065**, 706508 (2008).
- ²⁰F. Gervais and B. Piriou, *Phys. Rev. B* **10**, 1642 (1974).
- ²¹Z. Li, K. Aydin, and E. Ozbay, *Phys. Rev. E* **79**, 026610 (2009).